Filling Factor and Isolator Performance of the Traveling-Wave Maser*

By F. S. CHEN and W. J. TABOR

(Manuscript received December 16, 1963)

In designing a large gain and simultaneously large instantaneous bandwidth traveling-wave maser (TWM), the filling factor and the isolator performance should be optimized.

The filling factor is a measure of the efficiency of interaction between the spin system of the maser material and the RF magnetic fields of the slow-wave structure. For the TWM using the 90° operation of ruby and the comb as the slow-wave structure, the c axis of the ruby should be parallel to the z axis of the structure (the direction of the signal wave propagation) for the largest filling factor. The improvement of the filling factor by the proper orientation of the c axis of the ruby is larger at the lower signal frequencies because the transition probability of ruby is more nearly linear at those frequencies.

The isolator should provide sufficient reverse absorption to make the TWM short-circuit stable and yet add the minimum forward absorption to the TWM. Both the reverse and the forward absorption of the isolator depend critically on the size of the ferrite disks and the position in which they are imbedded in the comb structure.

An analysis of the filling factor and isolator performance and its comparison with measurements was made. Together with Refs. 1 and 2, this paper is intended to reduce the amount of experimental work involved in developing traveling-wave masers. Although the discussion is centered on the comb-type ruby TWM, the data provided also apply to other tape slow-wave structures using different active crystals.

I. INTRODUCTION

In order to make a large gain and simultaneously large instantaneous bandwidth traveling-wave maser (TWM), it is necessary to orient the

* This work was supported in part by the U. S. Army Signal Corps under Contract No. DA 36-039-SC-89169.

active material so that the susceptibility tensor has a maximum interaction with the RF magnetic field of the slow-wave structure. Quantitatively this is expressed as a filling factor, F, where:[1]

$$F = F_v F_p . \tag{1}$$

F_v is the volume filling factor and represents the fraction of the RF magnetic energy that is inside the active material. If all of the RF magnetic energy is within the boundaries of the active material, then this factor can have its maximum value of one. F_p is the phase filling factor and represents how well the RF field can couple to the susceptibility tensor of the active material. For example, if the active material is represented by a susceptibility with a transverse component of magnetization which is circularly polarized, and a structure with the RF magnetic field that is circular and in the same sense of rotation, then F_p is equal to one. It is clear therefore that the maximum value of the total filling factor F is one.

The present design for a TWM uses a comb structure that is loaded with active material on both sides and nearly fills all of the available space. There are, however, some regions that are not filled with active material; for example, the space occupied by the isolator, the space between the fingers, and the region near the wall of the waveguide housing that is important for the shaping of the ω-β response of the structure. However, these spaces are considered small, and therefore the volume filling factor is taken to be nearly one. Since the volume filling factor has nearly its maximum value, no further consideration will be made on F_v ; instead, our attention will be directed to F_p .

Since the comb structure has almost no RF fields in the direction of the fingers[2] and the ruby has no susceptibility component along the dc magnetic field when used in the 90° operation,[3] it is clear that the dc magnetic field must be placed parallel to the fingers of the comb for maximum efficiency. Therefore, the only degree of freedom for the c axis of the ruby is a rotation about an axis parallel to the fingers. In the comb structure the RF magnetic field changes with position and with θ, where θ is the phase difference between adjacent fingers of the structure and can have values from 0 to π over the passband of the structure. In addition, the susceptibility of the active material is a function of frequency. Hence F_p varies in a complicated fashion over the passband of the structure. It is our intention to find an expression of F_p as a function of the various dimensions of the structure, the angle between the c axis of the ruby and the z direction of the comb structure, and the phase difference θ.

The isolator incorporated in the comb structure consists of a linear array of ferrite disks arranged to have the same periodicity as the comb. The disks are so shaped that the ferrimagnetic resonance occurs at the same dc field and frequency as that required by the ruby. Two requirements of the isolator are: first, the isolator should provide reverse absorption at least equal to the round-trip gain provided by the ruby and second, the ratio of the reverse to forward attenuation should be high. Our objective in this part of the analysis is to find the effect of the various structural parameters of the comb on the performance of the isolator and to provide a guide toward the optimum design of the isolator. It is found that the structure that provides maximum gain performance is not the same as that for optimum isolator performance. Therefore, the attitude has been to design the structure for maximum gain performance and then to optimize the isolator within the constraints imposed by this structure.

In this paper, the attention will be centered on the comb as the slow-wave structure, a ferrimagnetic material such as YIG as the isolator, and ruby as the active material, where the latter is only considered in the 90° operation; i.e., the dc magnetic field is perpendicular to the crystalline c axis of the ruby. However, the analysis applies equally well to other types of taped structures and active materials, since the results are expressed as a function of θ and not of the frequency. The connection between the frequency and θ is made through the ω-β relations of the particular structure.

The assumption is made that the RF field configuration of the structure is unperturbed by the presence of the spin system of the ruby and the ferrite disks. This is justified, since the spins in ruby are very dilute and the ferrite disks are thin.

Under the following two conditions:[2] (i) no RF fields in the direction of the fingers and (ii) the field on that part of the z axis between the adjacent fingers independent of z (uniform field assumption), the RF magnetic fields in region 2 (see Fig. 1) can be expressed as:

$$H_z = j \sum_{n=-\infty}^{\infty} A_n \cosh \beta_n (D - x) e^{-j\beta_n z} \cos \frac{\pi y}{2h} \tag{2}$$

$$H_x = \sum_{n=-\infty}^{\infty} A_n \sinh \beta_n (D - x) e^{-j\beta_n z} \cos \frac{\pi y}{2h} \tag{3}$$

$$A_n = (-1)^n \sqrt{\frac{\epsilon_1}{\mu}} \frac{lE_0}{L} \frac{\sin \dfrac{\beta_n l}{2}}{\dfrac{\beta_n l}{2}} \frac{1}{\sinh \beta_n D} \tag{4}$$

$$\beta_n = \frac{\theta + 2n\pi}{L} \tag{5}$$

$$E_0 = -2j \frac{V_0}{l} \sin \frac{\theta}{2} \tag{6}$$

where the voltage on the mth finger is taken as $V_m = V_0 e^{-jm\theta}$, and h is the sum of the finger length and the correction due to the fringe capacitance at the finger tips. The rest of the notation is shown in Fig. 1. Equations (2) and (3) also assume $W = D$, which is a good approximation to the TWM with a large-gain, instantaneous-bandwidth product now in use.

Neglecting the copper and dielectric losses of the structure, the microwave signal power in the TWM can be expressed as:

$$P_o = P_i \exp\left[-\frac{L_T}{v_g} \frac{\omega \left\{ \int_m \mathbf{H} \cdot \chi_1'' \cdot \mathbf{H}^* \, dv + \int_i \mathbf{H} \cdot \chi_2'' \cdot \mathbf{H}^* \, dv \right\}}{\int_v \mathbf{H} \cdot \mathbf{H}^* \, dv} \right] \tag{7}$$

where P_i and P_o are the input and output power, respectively, L_T is the total length of the structure, v_g is the signal group velocity and χ_1'' and χ_2'' are the imaginary parts of the susceptibility tensor of the ruby and ferrite disks, respectively. The volume integral in the denominator with the subscript v encloses the whole volume of the structure per period, and the volume integrals in the numerator with the

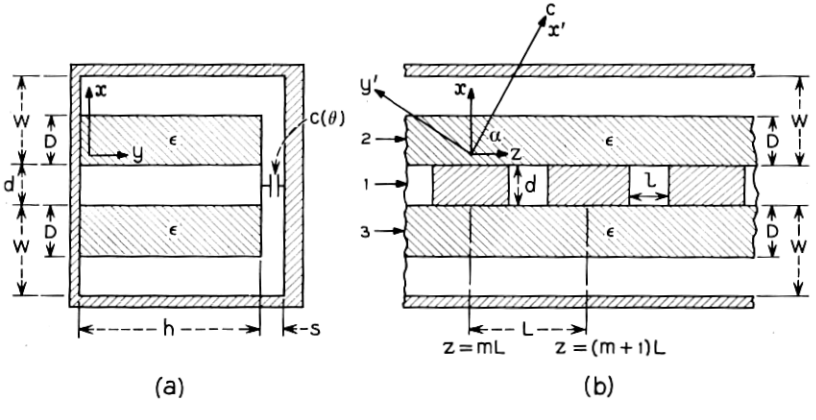

Fig. 1 — Comb structure loaded with ruby. The c axis of ruby makes an angle α with the z direction.

subscripts m and i enclose the volume of ruby or ferrite per period, respectively.

By performing the integration in (7) using the RF fields expressed in (2) and (3), the filling factor and the isolator performance can be found. The filling factor will be derived in Section II and the isolator performance will be discussed in Section III. In both sections the results of theory are compared with the measurements. In Section IV, concluding remarks will be made.

II. FILLING FACTORS

2.1 *Analysis and Discussions*

The susceptibility tensor in (7) is a classical expression, whereas the properties of ruby are given in terms of the spin Hamiltonian; it is therefore necessary to establish a connection between χ_1'' and the quantum mechanical properties of ruby. The subscript one will now be dropped from χ_1''. Throughout this paper MKS units will be used.

Classically, the absorbed power is given by

$$P_{\text{abs}} = \tfrac{1}{2}\mu_0\omega \int_m \mathbf{H}\cdot\chi''\cdot\mathbf{H}^* \, dv \tag{8}$$

where μ_0 is the permeability of free space, ω is the frequency in radians per second, and $\mathbf{H}$ is the RF magnetic field. The quantum mechanical expression for absorbed power is given by:

$$P_{\text{abs}} = \int_m W_{1\text{-}2}(\rho_1 - \rho_2)\hbar\omega \, dv \tag{9}$$

where ρ_1 and ρ_2 are the densities of spins in levels 1 and 2 respectively, $\hbar$ is Planck's constant divided by 2π, and $W_{1\text{-}2}$ is the transition probability between the levels in question. $W_{1\text{-}2}$ is in general a function of the position.

Equating (8) and (9) and dividing through by the total RF energy, $\mu_0\int_v \mathbf{H}\cdot\mathbf{H}^* dv$, one obtains:

$$\frac{\int_m \mathbf{H}\cdot\chi''\cdot\mathbf{H}^* \, dv}{\int_v \mathbf{H}\cdot\mathbf{H}^* \, dv} = \frac{2\int_m W_{1\text{-}2}(\rho_1 - \rho_2)\hbar \, dv}{\mu_0 \int_v \mathbf{H}\cdot\mathbf{H}^* \, dv}. \tag{10}$$

The left-hand side of (10) is exactly the expression occurring in (7).

One can further define:

$$F_v \equiv \frac{\int_m \mathbf{H}\cdot\mathbf{H}^*\,dv}{\int_v \mathbf{H}\cdot\mathbf{H}^*\,dv} \tag{11}$$

$$F_p \equiv \frac{\int_m \mathbf{H}\cdot\chi''\cdot\mathbf{H}^*\,dv}{(\chi_{x'x'}'' + \chi_{y'y'}'')\int_m \mathbf{H}\cdot\mathbf{H}^*\,dv} \tag{12}$$

where F_v and F_p are the volume and the phase filling factors, respectively, and $\chi_{x'x'}''$, $\chi_{y'y'}''$ are the diagonal elements of the susceptibility tensor. $\chi_{z'z'}''$ is not present in (12), since this term is zero for the 90° operation. The prime in the subscripts of χ'' refers to the crystal axes of ruby. The x' axis is taken parallel to the crystalline c axis. (see Fig. 1). In general, both the RF magnetic field and the spin magnetic moment have elliptic polarizations, and when these ellipses have the same sense of rotation, the same principal axes and the same shape (i.e., $H_x^2\chi_{yy}'' = H_y^2\chi_{xx}''$), then F_p as defined above has its maximum value of one. The actual value of F_p for the comb structure will then be a measure of how the fields depart from this ideal case.

Comparing (10), (11) and (12) one obtains:

$$F_p = \frac{2\int_m W_{1\text{-}2}(\rho_1 - \rho_2)\hbar\,dv}{\mu_0(\chi_{x'x'}'' + \chi_{y'y'}'')\int_m \mathbf{H}\cdot\mathbf{H}^*\,dv}. \tag{13}$$

It is now necessary to calculate the detailed expression for $W_{1\text{-}2}$. One starts with an unperturbed Hamiltonian $\mathcal{H}_0$ and the time-dependent Schrodinger equation

$$\mathcal{H}_0\psi = i\hbar(\partial\psi/\partial t) \tag{14}$$

whose solutions are $\psi_\lambda \exp -[(iE_\lambda/\hbar)t]$. For this calculation the ψ_λ eigenfunctions are those obtained from the spin Hamiltonian for ruby.[3] A perturbation term is now added which will represent the coupling of the spins in ruby to the RF magnetic field. If this perturbation is called $\mathcal{H}_1$, then the equation that must be solved is:

$$(\mathcal{H}_0 + \mathcal{H}_1)U = i\hbar(\partial U/\partial t) \tag{15}$$

where

$$\mathcal{H}_1 = \boldsymbol{\mu} \cdot \mathbf{H} \tag{16}$$

$\boldsymbol{\mu}$ is the magnetic moment of the spin, and $\mathbf{H}$ is the RF magnetic field. $\boldsymbol{\mu}$ is given by:

$$\boldsymbol{\mu} = g\beta\mathbf{S} \tag{17}$$

where g is the spectroscopic splitting factor, β is the Bohr electronic magneton, and $\mathbf{S}$ is the spin angular momentum operator.

The RF magnetic fields are given in (2) and (3). For convenience they can be expressed as:

$$H_z = \cos\frac{\pi y}{2h} \sum_n L_n(\theta,x) \left(-\frac{i}{2}\right) [\exp i(\omega t + \beta_n z) - \exp -i(\omega t + \beta_n z)] \tag{18}$$

$$H_x = \cos\frac{\pi y}{2h} \sum_n M_n(\theta,x) \left(\tfrac{1}{2}\right) [\exp i(\omega t + \beta_n z) + \exp -i(\omega t + \beta_n z)] \tag{19}$$

where

$$L_n = A_n \cosh \beta_n(D - x)$$

$$M_n = A_n \sinh \beta_n(D - x).$$

The coordinate system for the ruby and comb structure is shown in Fig. 1. For an angular separation of α between the z and x' axes, (16) becomes:

$$\mathcal{H}_1 = g\beta[(S_{x'} \sin\alpha + S_{y'} \cos\alpha)H_x + (S_{x'} \cos\alpha - S_{y'} \sin\alpha)H_z]. \tag{20}$$

Equation (15) will be solved in terms of an infinite series of unperturbed solutions ψ_λ, i.e.,

$$U = \sum_\lambda C_\lambda(t) \exp - [i(E_\lambda/\hbar)t] \tag{21}$$

where the expansion coefficients depend on the time. $|C_\lambda(t)|^2$ is the probability of finding the spin in the state ψ_λ at the time t. Initially the spin is assumed to be in the state ψ_1, i.e., $|C_1(0)|^2 = 1$, $|C_\lambda(0)|^2 = 0$ for $\lambda > 1$. The perturbation is then turned on and a solution for $|C_2(t)|^2$ is sought. $|C_2(t)|^2$ is the probability of finding the spin in state 2. For weak RF magnetic fields this term is equal to:

$$|C_2(t)|^2 = W_{1\text{-}2}t. \tag{22}$$

The process of obtaining $|C_2(t)|^2$ is a standard one in quantum

mechanics[4] and will not be given in detail here. The result is

$$\mathbf{W}_{1\text{-}2} = \frac{g^2\beta^2\pi}{2\hbar^2}\, g(\omega - \omega_0) \sum_{n,m} (O_n O_m + P_n P_m) \tag{23}$$

where $g(\omega - \omega_0)$ is a normalized line shape function such that:

$$\int_{-\infty}^{\infty} g(\omega - \omega_0)\, d\omega = 1$$

and

$$\begin{aligned} O_n &= (\langle S_{y'}\rangle M_n + \langle S_{x'}\rangle L_n) \cos\alpha \cos\beta_n z \\ &\quad - (\langle S_{x'}\rangle M_n + \langle S_{y'}\rangle L_n) \sin\alpha \sin\beta_n z \\ P_n &= (\langle S_{x'}\rangle M_n + \langle S_{y'}\rangle L_n) \sin\alpha \cos\beta_n z \\ &\quad + (\langle S_{y'}\rangle M_n + \langle S_{x'}\rangle L_n) \cos\alpha \sin\beta_n z \end{aligned}$$

$$\langle S_{x'}\rangle \equiv \int \psi_1 S_{x'} \psi_2^*\, dv, \qquad \langle S_{y'}\rangle \equiv \int \psi_1 S_{y'} \psi_2^*\, dv.$$

Substituting (23) into (12), one obtains:

$$F_p = \frac{g^2\beta^2\pi g(\omega - \omega_0)(\rho_1 - \rho_2) \int \sum_{n,m} (O_n O_m + P_n P_m)\, dv}{\hbar\mu_0(\chi_{x'x'}'' + \chi_{y'y'}'') \int \mathbf{H}\cdot\mathbf{H}^*\, dv}. \tag{24}$$

If we were to examine just one element of the χ'' tensor, say $\chi_{x'x'}''$, and subject it to a simple field, $H_{x'} \sin \omega t$, then by going through the same procedure [using (13)–(22)] one could establish that:

$$\chi_{x'x'}'' = \frac{g^2\beta^2\pi}{\mu_0\hbar}\, g(\omega - \omega_0)(\rho_1 - \rho_2)\, |\langle 1 \mid S_{x'} \mid 2\rangle|^2 \tag{25}$$

and similarly for the other elements in the tensor.

Using (25) to simplify (24), one obtains:

$$F_p = \frac{\int_m \sum (O_n O_m + P_n P_m)\, dv}{(\langle S_{x'}\rangle^2 + \langle S_{y'}\rangle^2) \int_m \mathbf{H}\cdot\mathbf{H}^*\, dv}. \tag{26}$$

The phase filling factor will now be calculated for two cases: (1) a ruby TWM loaded on one side and (2) a ruby TWM loaded on both sides. In both cases it is assumed that the ruby entirely fills the gap between the fingers and the outer waveguide wall and extends to the

open tip of the fingers. In addition, it is assumed that, in the case of a TWM loaded with ruby on one side only, the opposite side is still filled with a material whose dielectric constant equals that of ruby. In practice this assumption is fulfilled very closely with recently developed masers.[5] By performing the integration in (26), one obtains

$$F_p(\tfrac{1}{2}) = \tfrac{1}{2} \pm \frac{\langle S_{x'}\rangle\langle S_{y'}\rangle}{\langle S_{x'}\rangle^2 + \langle S_{y'}\rangle^2} \sum (\tfrac{1}{2}) + \frac{[\langle S_{x'}\rangle^2 - \langle S_{y'}\rangle^2] \cos 2\alpha}{2[\langle S_{x'}\rangle^2 + \langle S_{y'}\rangle^2]} \sum (1) \tag{27}$$

for the structure filled on one half side, and

$$F_p(1) = \tfrac{1}{2} + \frac{[\langle S_{x'}\rangle^2 - \langle S_{y'}\rangle^2] \cos 2\alpha}{2[\langle S_{x'}\rangle^2 + \langle S_{y'}\rangle^2]} \sum (1) \tag{28}$$

for the completely filled structure. $\sum (\frac{1}{2})$ and $\sum (1)$ are defined as follows:

$$\sum (\tfrac{1}{2}) = \frac{\sum \frac{E_0^2}{\beta_n D} \frac{\sin^2\left(\frac{\beta_n l}{2}\right)}{\left(\frac{\beta_n l}{2}\right)^2}}{\sum \frac{E_0^2}{\beta_n D} \frac{\sin^2\left(\frac{\beta_n l}{2}\right)}{\left(\frac{\beta_n l}{2}\right)^2} \frac{\cosh \beta_n D}{\sinh \beta_n D}} \tag{29}$$

$$\sum (1) = \frac{\sum \frac{E_0^2}{\beta_n D} \frac{\sin^2\left(\frac{\beta_n l}{2}\right)}{\left(\frac{\beta_n l}{2}\right)^2} \frac{1}{\sinh^2 \beta_n D}}{\sum \frac{E_0^2}{\beta_n D} \frac{\sin^2\left(\frac{\beta_n l}{2}\right)}{\left(\frac{\beta_n l}{2}\right)^2} \frac{\cosh \beta_n D}{\sinh \beta_n D}}. \tag{30}$$

The $\pm$ sign of the second term in (27) determines the nonreciprocal behavior of the ruby TWM. In the direction of propagation where the elliptically polarized fields of the comb structure are in the same sense as the near circular transition of ruby, the plus sign applies. In the opposite direction, where the fields are not as well matched, the minus sign applies.

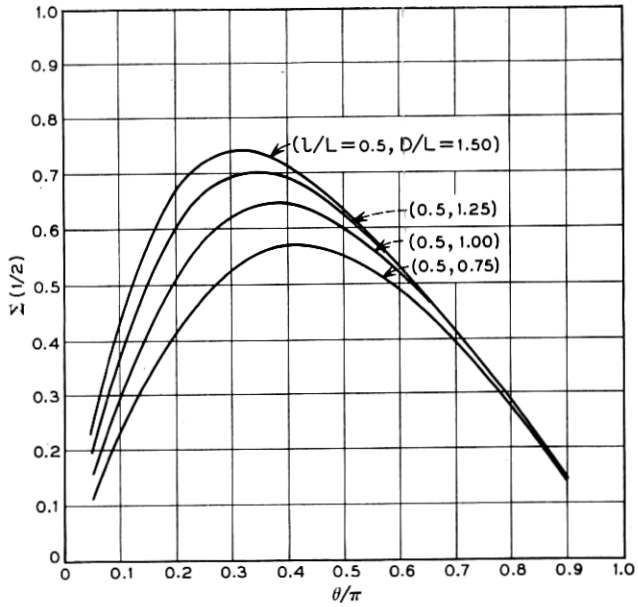

Fig. 2 — $\Sigma(\frac{1}{2})$ vs θ/π for $l/L = 0.5$ and four values of the parameter D/L.

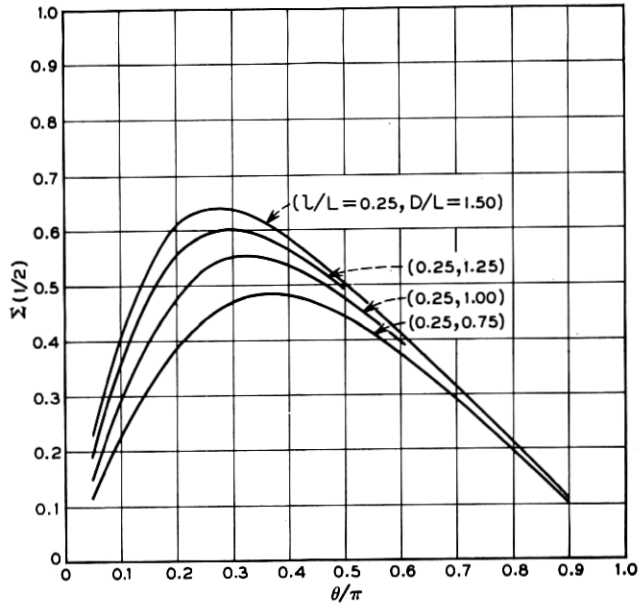

Fig. 3 — $\Sigma(\frac{1}{2})$ vs θ/π for $l/L = 0.25$ and four values of the parameter D/L.

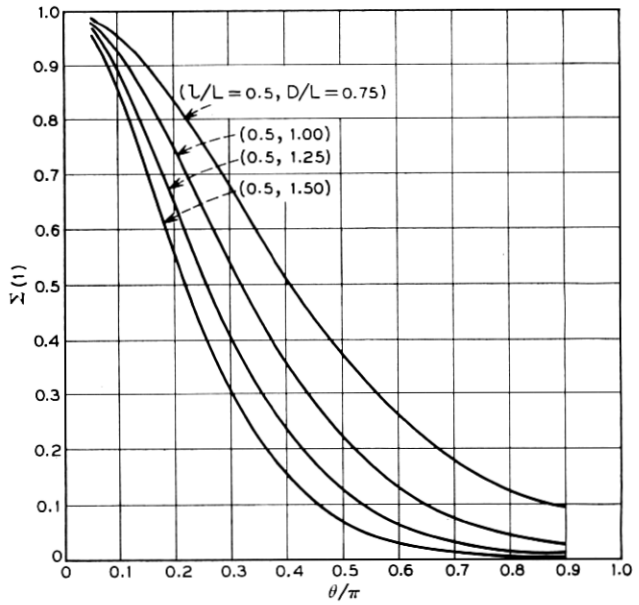

Fig. 4 — $\Sigma(1)$ vs θ/π for $l/L = 0.5$ and four values of the parameter D/L.

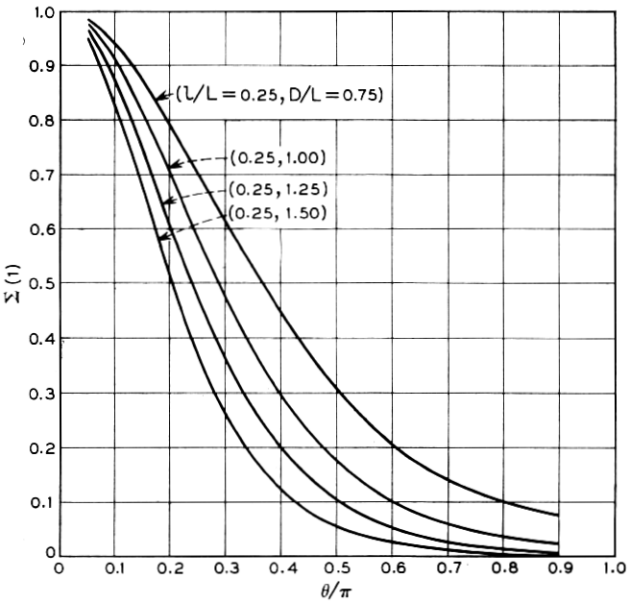

Fig. 5 — $\Sigma(1)$ vs θ/π for $l/L = 0.25$ and four values of the parameter D/L.

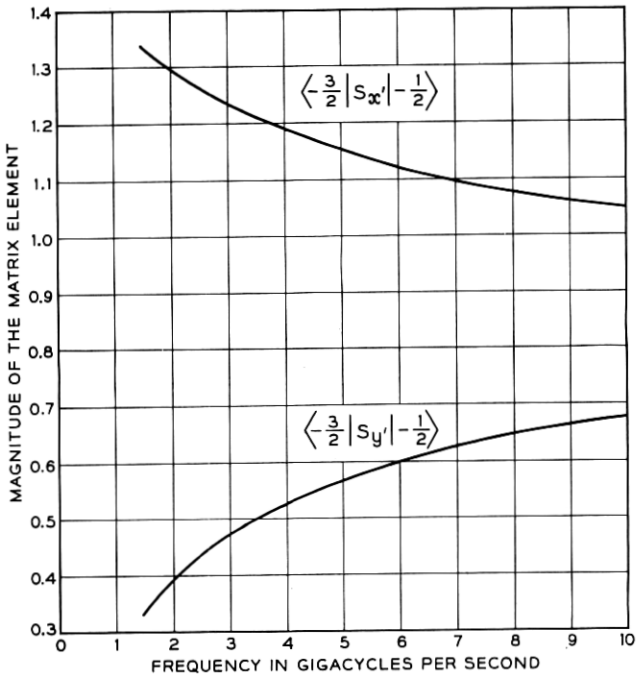

Fig. 6 — A plot of $\langle S_{x'} \rangle$ and $\langle S_{y'} \rangle$ as functions of frequency.

The $\sum$'s are in general functions of the parameters l/L, and D/L and θ, where the terms l, L and D are defined in Fig. 1. $\sum(\frac{1}{2})$ and $\sum(1)$ are plotted as a function of θ in Figs. 2, 3, 4 and 5. Fig. 6 is a plot of the absolute values of the matrix elements, $\langle S_{x'} \rangle$ and $\langle S_{y'} \rangle$, as a function of frequency. The matrix elements are calculated between the levels $-\frac{3}{2} \leftrightarrow -\frac{1}{2}$ for the 90° operation of ruby. With the data presented in Figs. 2 to 6 and (27) and (28), the phase filling factor for a ruby loaded comb structure can be closely estimated.

Equation (28) shows that the phase filling factor for the completely filled structure is $\frac{1}{2}$ if the transition probability of the ruby is circular (i.e., $\langle S_{x'} \rangle = \langle S_{y'} \rangle$) regardless of the angle α, or, if $\alpha = \pi/4$ radians, regardless of the ratio $\langle S_{x'} \rangle / \langle S_{y'} \rangle$. This can be shown to be the consequence of the symmetry of the RF magnetic fields about the plane of the fingers. Equation (28) also shows that the filling factor does not depend on the sign of α, i.e., cos 2α is an even function of α. This result is a consequence of the symmetry of the RF fields about a plane parallel to the x-y plane and centered between the fingers.

The filling factor increases as D/L becomes smaller (see Fig. 3) if $\langle S_x' \rangle$ is greater than $\langle S_y' \rangle$. This is due to the fact that the RF magnetic fields become more linear as D/L gets smaller.

The ratio of the electronic gain of the TWM with both sides loaded with ruby to that with only one side loaded with ruby is shown as a function of θ for different frequencies in Fig. 7. The curves are obtained assuming $D/L = 0.75$, $l/L = 0.5$ and $F_v = 0.5$ for a half loaded and $F_v = 1.0$ for a fully loaded comb. Even at 10 gc, where the transition probability of the ruby is becoming fairly circular, a 30 per cent increase in gain can be obtained by loading the second side with ruby. As an example, let us consider a structure with 30 db electronic gain when the ruby is loaded on one side only. The round-trip gain would be $30 + 0.3(30) = 39$ db, (assuming $\theta = \pi/2$). An isolator of at least 39 db would be required to assure short-circuit stability, and since the reverse-to-forward loss ratio of an isolator is about 20, the forward loss of the isolator would be approximately 2 db. If the structure were now loaded on both sides, the forward gain would increase to 39 db and the round-trip gain would be 78 db. The forward loss of the isolator

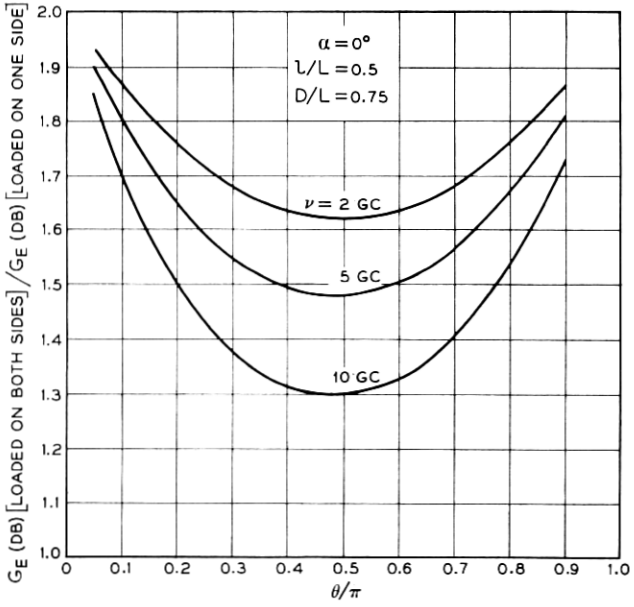

Fig. 7 — The ratio of the electronic gain (in db) of a maser when loaded on both sides to that when loaded on one side. The structures are otherwise identical, with $\alpha = 0°$, $l/L = 0.5$, $D/L = 0.75$.

for this structure would be approximately 4 db. The net gain (excluding the common copper loss) is therefore 28 db for the single-sided loading and 35 db for the double-sided case. It is therefore clear that two-sided loading is more efficient at least up to X-band, although not by a very large margin.

2.2 *Experimental Verification*

Equation (27) was checked experimentally by measuring the paramagnetic absorption in a structure loaded on one side with ruby. The other side of the comb structure was loaded with alumina which has about the same dielectric constant as ruby. The measurements were performed in absorption so that complicating factors such as a microwave pump and isolator could be avoided. Equation (7), of course, defines the absorbed power as well as the gain of the TWM. The passband of the structure was centered at approximately 5.4 gc. Since (27) is a function of the angle between the c axis of the ruby and the z direction of the structure α, two different pieces of ruby were used: one with $\alpha = 67°$ and another with $\alpha = 20°$.

In the evaluation of F_p the volume filling factor, F_v, was taken to be exactly $\frac{1}{2}$. All the measurements that enter into (7) were performed at 4.2°K. v_g was calculated from the ω-β response of the structure. The ω-β plot was obtained by a bridge technique in which the difference in path length of the two arms of the bridge was carefully accounted for and subtracted from the measurement. In this way, the correct ω-β response of the comb structure was assured.

The term $(\rho_1 - \rho_2)$ that enters into the susceptibility formula (25) is difficult to determine exactly, since it depends on the chemical analysis of the ruby. Since the major concern of this experiment is the filling factor and not the accuracy of the chemical analysis, the concentration was left as a parameter to be used as a best fit to the calculated value of F_p. The assumed concentration was then compared with that obtained by chemical analysis.[6]

Figs. 8 and 9 are plots of the experimentally measured and calculated values of F_p. Table I compares the assumed concentration to that obtained by chemical analysis.

Figs. 8 and 9 both show the same type of behavior. The ratio of experimentally measured values to the calculated values decreases as θ increases. Part of this may be explained by the fact that the value of the volume filling factor, F_v, was taken to be exactly $\frac{1}{2}$ for all values of θ. This is a good approximation when $\theta = 0°$, since no RF fields exist between the fingers, but at large values of θ, RF fields do exist between

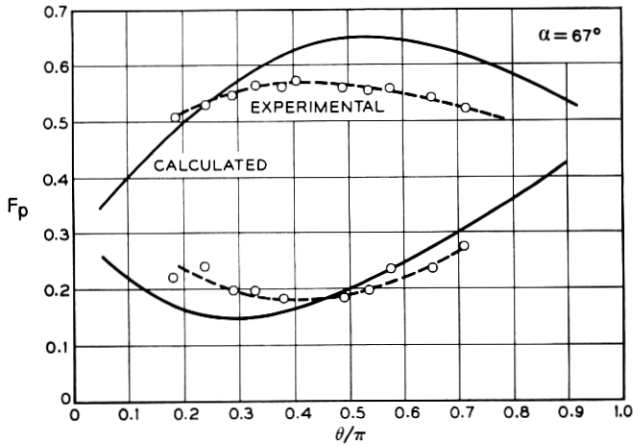

Fig. 8 — A comparison of the theoretical and experimental results for a ruby with $\alpha = 67°$. The solid line is the theoretical curve and the points are the experimental measurements.

fingers where there is no ruby, and therefore $F_v < \frac{1}{2}$. If F_v becomes less than $\frac{1}{2}$, the experimentally determined value of F_p would correspondingly increase and approach the calculated one.

The assumed chromium concentrations compare very well with those determined by chemical analysis. In fact, in the case where $\alpha = 20°$

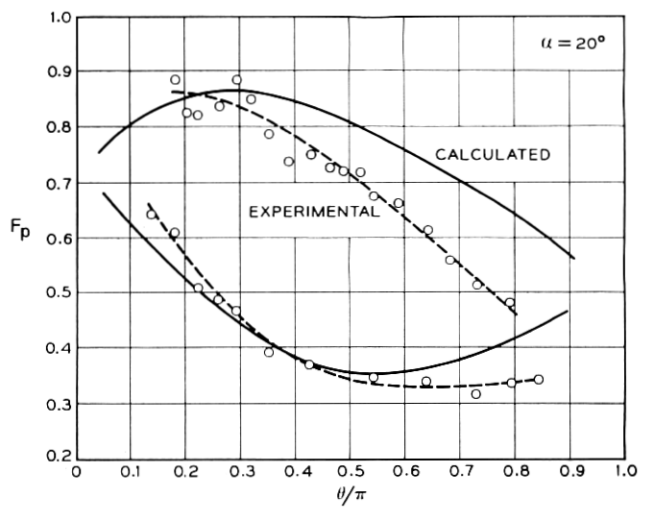

Fig. 9 — A comparison of the theoretical and experimental results for a ruby with $\alpha = 20°$. The solid line is the theoretical curve and the points are the experimental measurements.

TABLE I — COMPARISON OF ASSUMED CONCENTRATION TO CONCENTRATION DETERMINED BY CHEMICAL ANALYSIS

α	Assumed Conc. (Cr/Al Atomic %)	Chemical Analysis (Cr/Al Atomic %)
67°	0.032	0.030
20°	0.028	0.028

the concentrations are the same and therefore Fig. 9 can be considered to be free of all adjustable parameters. However, the concentrations determined by chemical analysis cannot be considered highly accurate on an absolute basis, and therefore this agreement could be fortuitous.

III. ISOLATOR PERFORMANCES

The isolator consists of thin ferrite disks imbedded periodically inside the ruby slab as shown in Fig. 10. The dc magnetic field is applied in the y direction, and it is normal to the plane of the ferrite disks. The ferrite disks are usually thin and have square cross sections. The ratio of the side dimension to the thickness of the square (aspect ratio) is so adjusted that the ferrite resonates at the same dc magnetic field as ruby for a given frequency.

In Section 3.1, the analysis and the result of the machine computation will be presented. The calculation is compared with the measurements in Section 3.2.

3.1 *Analysis and Discussion*

Since the dielectric constant of the ferrite is about the same as the surrounding ruby, the ferrite disks are thin, and the plane of the precessing spins coincides with the plane of the RF magnetic field before the introduction of the ferrite disks, then the disturbance of the RF fields due to the presence of the resonating ferrite disks should be small.

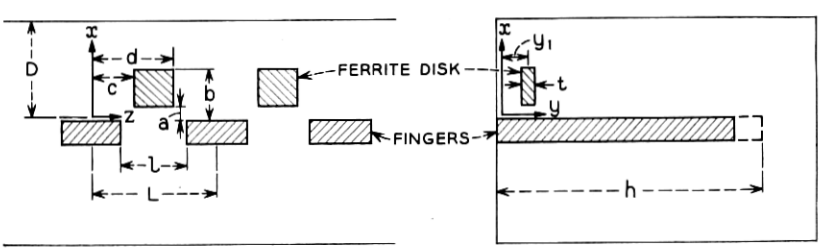

Fig. 10 — Ferrite disk isolators imbedded in the comb structure.

Perturbation theory, which assumes the RF fields inside the ferrite to be the same as those present if the ferrite were replaced by the ruby, should be appropriate for the analysis here.

We shall regard the ferrite square block as an approximation to an ellipsoid. Then the demagnetization factors N_x, N_y and N_z in the x, y and z directions, respectively, can be defined in the usual manner. In this approximation, the demagnetization factor of a square disk will be approximated by the demagnetization factor of a circular disk, i.e., $N_x = N_z$. Even if the disk is not square, $N_x \approx N_z \approx 0$ if the disk is sufficiently thin. In such cases, the imaginary part of the external susceptibility tensor χ_2'' becomes diagonal when the RF fields are expressed in circular components.

From (2) and (3), the positive and negative circular components of the RF magnetic field can be defined as

$$H_+ \equiv \frac{1}{\sqrt{2}}(H_x - jH_z) = \frac{j}{\sqrt{2}} \sum_{n=-\infty}^{\infty} A_n e^{\beta_n(D-x)} e^{-j\beta_n z} \cos \frac{\pi y}{2h} \tag{31}$$

$$H_- \equiv \frac{1}{\sqrt{2}}(H_x + jH_z) = \frac{j}{\sqrt{2}} \sum_{n=-\infty}^{\infty} A_n e^{-\beta_n(D-x)} e^{-j\beta_n z} \cos \frac{\pi y}{2h}. \tag{32}$$

Let χ_+'' and χ_-'' be the diagonal elements of the diagonalized χ_2''. They can be expressed as[7]

$$\chi_+'' = \frac{\omega_m T^{-1}}{(\omega_e - \omega)^2 + T^{-2}} \tag{33}$$

$$\chi_-'' = \frac{\omega_m T^{-1}}{(\omega_e + \omega)^2 + T^{-2}} \tag{34}$$

$$\omega_e = \gamma[H_0 + (N_x - N_y)4\pi M] \tag{35}$$

$$\omega_m = \gamma 4\pi M \tag{36}$$

$$T = \frac{2}{\gamma \Delta H}, \qquad \gamma = 2.8 \text{ mc/oe} \tag{37}$$

where $4\pi M$ is the saturation magnetization, H_0 is the externally applied dc magnetic field and ΔH is the linewidth of the ferrite. In terms of the circular components the absorption due to the ferrite is given by [see (7)]

$$\alpha_+ = \frac{\omega L_T}{v_g} \cdot \frac{\chi_+'' \int_i H_+ H_+^* \, dv + \chi_-'' \int_i H_- H_-^* \, dv}{\int_v (H_+ H_+^* + H_- H_-^*) \, dv} \text{ neper} \tag{38}$$

$$\alpha_- = \frac{\omega L_T}{v_g} \frac{\chi_+'' \int_i H_- H_-^* \, dv + \chi_-'' \int_i H_+ H_+^* \, dv}{\int_v (H_+ H_+^* + H_- H_-^*) \, dv} \text{ neper} \quad (39)$$

where α_+ and α_- are the reverse and the forward absorption of the isolator, respectively. For most of the ferrites used in TWM's, $\chi_-'' \ll \chi_+''$. Therefore, the terms containing χ_-'' can be neglected. Substituting (31) and (32) into (38) and (39) and performing the integrations, one obtains

$$\alpha_\pm = 27.3 \frac{L_T}{v_g} \left(\frac{f}{Q_\pm} \right) \text{db} \quad (40)$$

where f is the frequency and $Q_\pm$ is defined as

$$1/Q_+ = t/h \, [\cos (\pi y_1/2h)]^2 \, \chi_+'' \, A \quad (41)$$

$$1/Q_- = t/h \, [\cos (\pi y_1/2h)]^2 \, \chi_+'' \, B. \quad (42)$$

A and B are ratios of the energy of the RF magnetic field due to the positive and the negative circular components over the area occupied by the ferrite disk to the total RF magnetic field energy contained over the area in the x-z plane per period, respectively. They can be expressed as

$$\left.\begin{matrix} A \\ B \end{matrix}\right\} = \frac{1}{\sum_{n=-\infty}^{\infty} |A_n|^2 \frac{\sinh 2\beta_n D}{2\beta_n D}} \times \sum_{m=-\infty}^{\infty} \sum_{n=-\infty}^{\infty} A_n A_m^* \frac{\sin \frac{(\beta_m - \beta_n)(d-c)}{2} \cos \frac{(\beta_m - \beta_n)(d+c)}{2}}{(\beta_m^2 - \beta_n^2) \, LD} \times [\exp \pm(\beta_m + \beta_n)(D-a)][\pm 1 \mp \exp \mp(\beta_m + \beta_n)(b-a)] \quad (43, 44)$$

where the upper and the lower signs are for A and B respectively. The notations a, b, c and d are defined in Fig. 10. In (43) and (44), the RF field energy contained in the region between the fingers (region 1 in Fig. 1) is neglected, since this is usually small compared to the RF field energy contained in the ruby.

Equations (43) and (44) were computed and the results are shown in Figs. 11–14. Note that A is a quantity proportional to the reverse absorption and A/B is the ratio of the reverse to the forward absorption of the isolators. Large A and A/B over a large range of θ are desirable

for the isolators. Since Figs. 11–14 are shown in terms of θ/π rather than the frequency, the frequency-phase relation (ω-β diagram) of the structure has to be known in order to convert θ into the frequency. All the dimensions involved were normalized by the length of a period of the structure L. In order to provide an easier understanding of the numerical data, we shall assume $L = 0.08$ inch (the commonly used size in our laboratory) and discuss the data with the parameters expressed in inches.

Since the isolation ratio becomes worse when the width of the waveguide housing gets narrower, we shall study the structure with small D first ($D/L = 0.75$). In Fig. 11, A and A/B vs θ/π are shown when

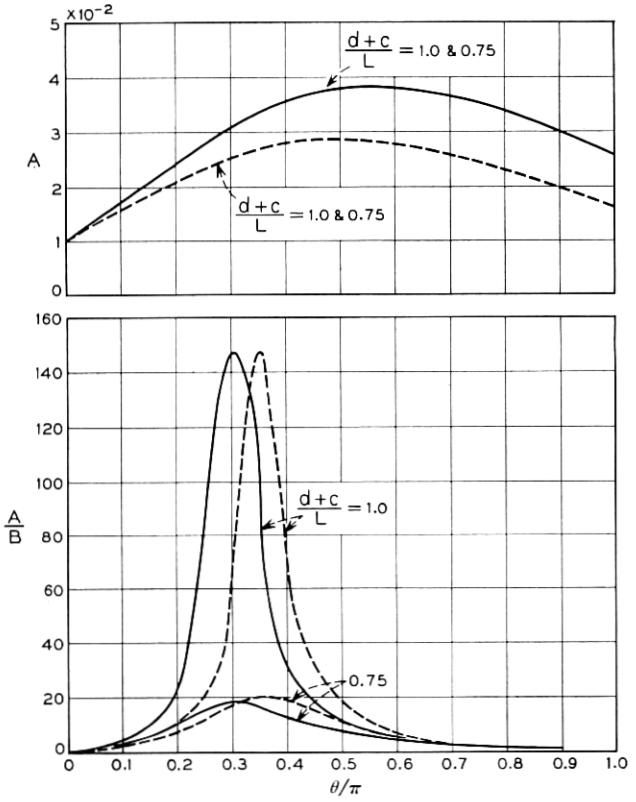

Fig. 11 — A and A/B vs θ/π for the following parameters: $D/L = 0.75$, $l/L = 0.5$; ferrite size, $(b - a)/L = (d - c)/L = 0.125$ (0.01 × 0.01 inch); solid curves for $(D - a)/L = 0.6875$ ($a = 0.005$ inch); broken curves for $(D - a)/L = 0.625$ ($a = 0.01$ inch).

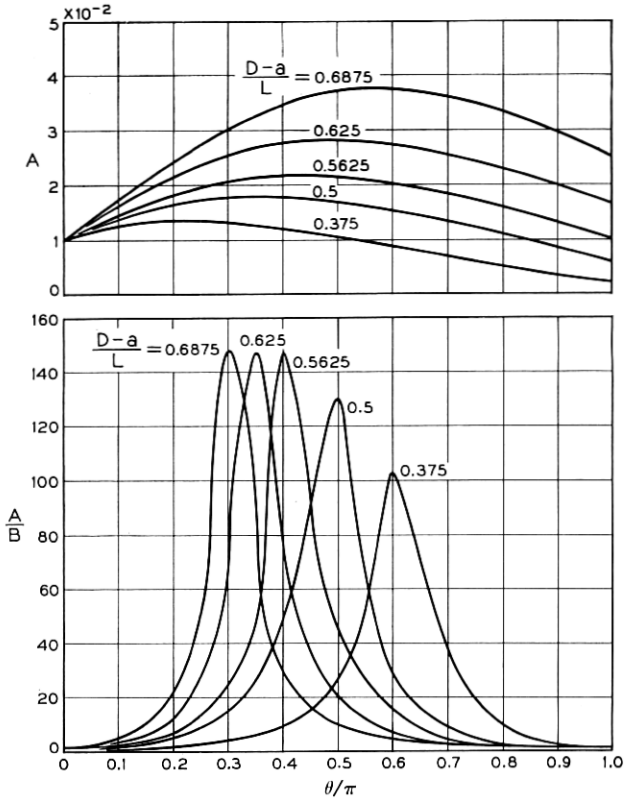

Fig. 12 — A and A/B vs θ/π for the following parameters: $D/L = 0.75$, $l/L = 0.5$; ferrite size, $(b - a)/L = (d - c)/L = 0.125$ (0.01 × 0.01 inch); $(d + c)/L = 1.0$ (ferrite on an axis midway between the adjacent fingers).

ferrite disks of 0.01 × 0.01 inch are placed in different positions of the structure. Solid lines are for the case where one edge of the disk is 0.005 inch away from the surface of the fingers, i.e., $a = 0.005$ inch (see Fig. 10). If the center of the disk is exactly at the position midway between the adjacent fingers $[(d + c)/L = 1.0]$, the isolation ratio A/B can be as large as 140 over a small range of θ. If the disk is shifted in the z direction by 0.01 inch $[(d + c)/L = 0.75]$, the isolation ratio decreases to values less than 20 while A remains almost the same. Next, let us take $a = 0.01$ inch (see the broken lines). At the position $(d + c)/L = 1.0$, the isolation ratio again reaches over 140. Again, shifting the position in the z direction by 0.01 inch decreases the isolation ratio to about 20. One sees readily that the isolator disks have to be positioned carefully

at the position midway between the adjacent fingers. A small displacement from this position deteriorates the isolation ratio rapidly. This has been known experimentally for a long time, and indeed the position of the largest A/B for a given a dimension is found in practice by moving the bar imbedded periodically with the isolator disks until the minimum forward attenuation results. Hence we shall assume the center of the ferrite disk to be on the line midway between the adjacent finger ($z = L/2$) in all of the following discussions.

Next, let us consider how the isolator performs as a is increased further. Fig. 12 shows A and A/B vs θ/π for 0.01 × 0.01 inch isolator disk as a is increased to 0.005, 0.01, 0.015, 0.02 and 0.03 inch [corre-

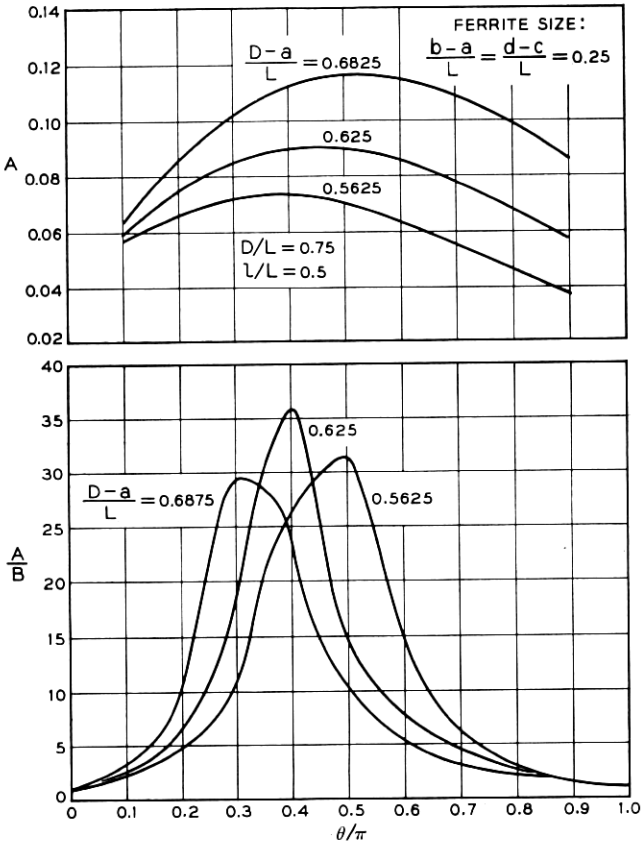

Fig. 13 — A and A/B vs θ/π: $D/L = 0.75$, $l/L = 0.5$; ferrite size, $(b - a)/L = (d - c)/L = 0.25$ (0.02 × 0.02 inch).

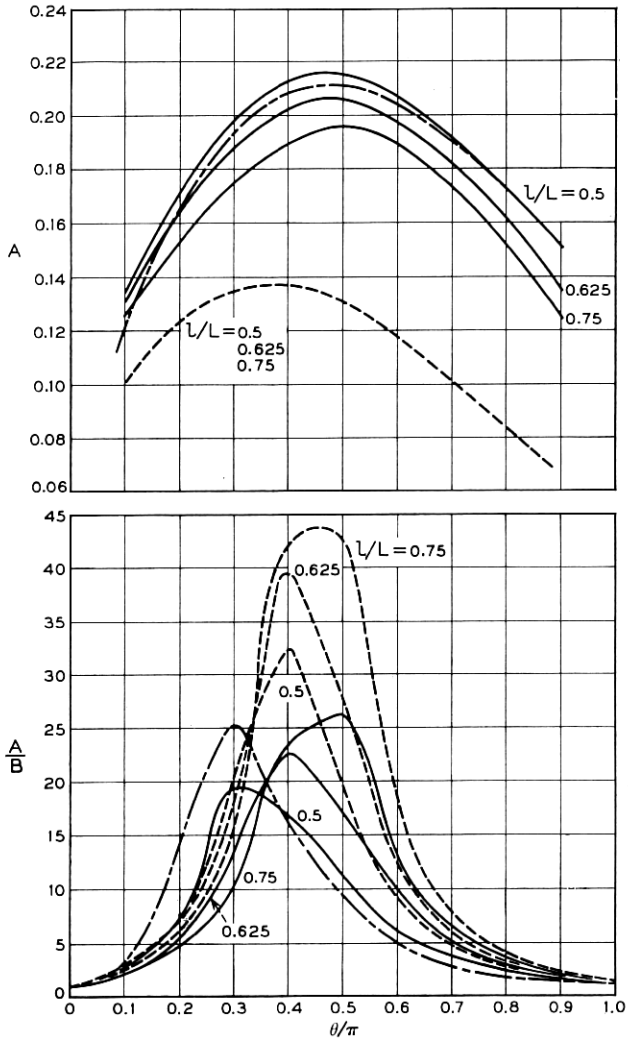

Fig. 14 — A and A/B vs θ/π: ferrite size, $(b - a)/L = (d - c)/L = 0.375$ (0.03 × 0.03 inch); solid line, $D/L = 0.75$, $(D - a)/L = 0.6875$ ($a = 0.005$ inch); dashed line, $D/L = 1.0$, $(D - a)/L = 0.8125$ ($a = 0.015$ inch); irregular dashed line, $D/L = 1.0$, $(D - a)/L = 0.9375$ (a = 0.005 inch); $l/L = 0.5$.

sponds to $(D - a)/L = 0.6875, 0.625, 0.5625, 0.5, 0.375$]. The maximum isolation ratio A/B is about the same from a = 0.005 to 0.015 inch and then it decreases for a larger a. This can be understood by noting that the RF magnetic field becomes linearly polarized at the wall of the waveguide housing, and hence A/B approaches one if the ferrite disk is placed near the wall. The value of θ at which the maximum A/B occurs gradually increases with the increase in a. If this were not so, a large value of A/B would still be maintained for ferrite disks of a larger cross section. Due to the spread of the peaks of A/B the ferrite disks of a larger cross section give small values of A/B. Larger values of a also reduce the reverse absorption (smaller A) since the RF energy is concentrated near the fingers.

In practice, the isolator disks of 0.01 × 0.01 inch cross section are too small to fabricate and also too small to provide enough reverse absorption. In order to see to which direction the size of the ferrite disks should be enlarged, let us consider two rectangular disks of 0.01 × 0.03 inch. One of them has a longer side parallel to the z axis and the other has a shorter side parallel to the z axis. Both disks have $a = 0.005$ inch. Then one can show from Figs. 11 and 12 that for the former case $A = 9 \times 10^{-2}$, $B = 3.2 \times 10^{-3}$ at $\theta = 0.3\pi$ where A/B is maximum, and for the latter case $A = 8.1 \times 10^{-2}$, $B = 1.08 \times 10^{-3}$ at $\theta = 0.35\pi$ where A/B is maximum. Apparently the latter is the better way to place rectangular ferrite disks.

Fig. 13 shows A and A/B vs θ/π for the ferrite disks of 0.02 × 0.02 inch. The edge of the ferrite disks is placed $a = 0.005$, 0.01 and 0.015 inch away from the surface of the fingers. As the ferrite disks are moved away from the surface of the fingers, the isolation ratio improves and then gets worse again. The reverse absorption steadily decreases at the same time. The sharp reduction of the isolation ratio by enlarging the size of the ferrite disks can be understood from the following considerations. At a given θ (or frequency), part of the ferrite disk at the position where B is small contributes little to the forward absorption, while the rest, located at the position where B is large, absorbs much of the forward-wave energy. Hence the forward absorption of the whole ferrite disk is larger. In another words, the peaks of A/B vs θ/π curve occurs at a different θ/π for different portions of the ferrite disk (see Fig. 12) The ferrite disks of this size are still not large enough to provide sufficient isolation for the high electronic gain attainable in present TWM's.

Fig. 14 shows A and the isolation ratio A/B vs θ/π when the size of the ferrite is increased to 0.03 × 0.03 inch (see the solid lines). The constant A increases almost twice from the value for 0.02 inch square

ferrite. Assuming the thickness of the ferrite $t = 0.1\ (d - c)$ (aspect ratio of 10), the reverse absorption of the isolator increases about 2×1.5 by increasing the size of the disk from 0.02 inch square to 0.03 inch square. However, the isolation ratio reduces from the maximum of 29.5 to 19.5 (the forward absorption increases 4.5 times).

It is clear by now that the isolation ratio of the isolator improves rapidly as the size of the ferrite disks gets smaller. On the other hand, the size of the ferrite has to be large to provide enough reverse absorption. Thus in order to improve the performance of the isolator, one faces contradicting requirements. One approach to circumvent this difficulty is to look for a ferrite of much larger susceptibility. Another solution is to look for a proper dimension of the structure to provide a larger area of circular polarization of the RF magnetic field. In Fig. 14 A and A/B vs θ/π are shown with a larger spacing between the fingers (ferrite size is 0.03 inch square). It is increased from $l = 0.04$ to 0.05 and to 0.06 inch while L is kept at 0.08 inch. The isolation ratio improves gradually.

Next consider the effect on the isolator performance when D/L is increased from 0.75 to 1.0. This will in general increase the group velocity.[2] From (7) and (40), the net db gain of TWM G_n is

$$G_n \propto \frac{1}{v_g}\left(F \mid \chi'' \mid - \frac{1}{Q_-}\right) \tag{45}$$

where F is the filling factor and $\mid \chi'' \mid$ is the susceptibility of the inverted spin system of the ruby. For the TWM to be short-circuit stable,

$$1/Q_+ > 2F \mid \chi'' \mid . \tag{46}$$

The isolator incorporated in the TWM should satisfy the condition (46) first, and then comes the consideration of how to reduce $1/Q_-$. The change in v_g will change the net gain and the reverse and the forward isolator absorption but not the stability condition (46). Hence, we shall confine our discussion here to the effect of $Q_\pm$ as D/L is increased. Suppose the condition (46) is satisfied with the isolator of $0.03 \times 0.03 \times 0.003$ inch, $a = 0.005$ inch, $l/L = 0.5$ and $D/L = 0.75$. If D/L is increased to 1.0, one sees from the irregular dashed curves in Fig. 14 that A remains almost the same, while the ruby filling factor reduces (see Fig. 4). Thus the TWM is still stable. However, the isolation ratio A/B increases from 19.5 to 25 (i.e., $1/Q_-$ decreases). Therefore the isolator performs better with larger D/L. Unfortunately, D/L is usually made small to provide a small group velocity near the center of the passband instead of being sized for the consideration of the

optimum isolator performance. Even if the forward absorption of the isolator increases with a smaller D/L, the net gain of the TWM may increase.

3.2 *Comparison of the Calculation with Measurements*

Isolators of 0.02 × 0.02 × 0.002 and 0.03 × 0.03 × 0.003 inch polycrystalline YIG disks were made and imbedded inside the comb structure of the dimensions shown in Fig. 15. The forward and the

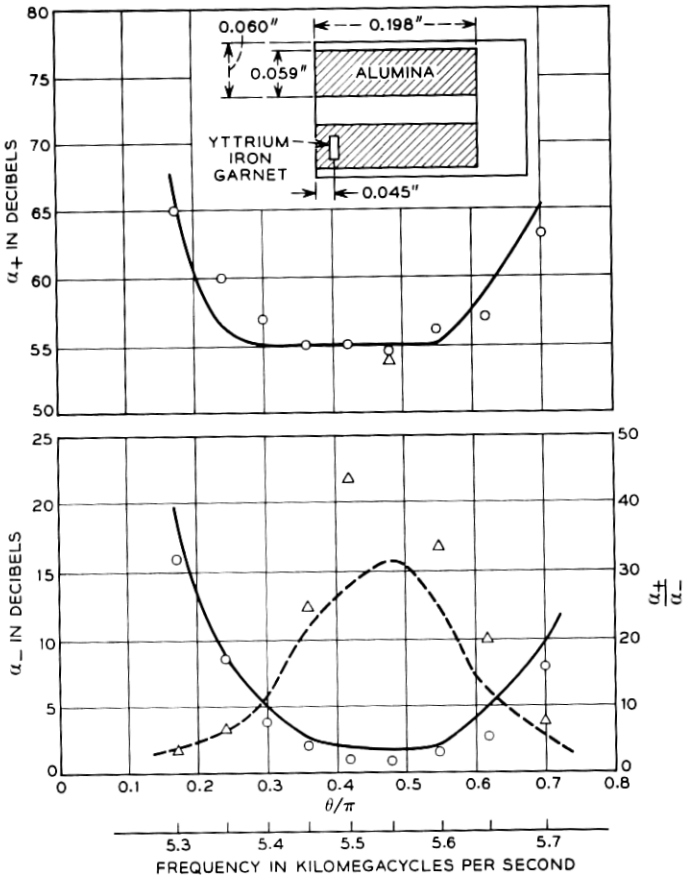

Fig. 15 — Measured and calculated forward and reverse losses. Ferrite disks 0.02 × 0.02 × 0.002 inch (71 pieces). L = 0.08 inch, D = 0.06 inch, l = 0.04 inch, a = 0.016 inch, ΔH = 223 oe, $4\pi M$ = 1750 oe. Solid lines are the calculated $\alpha_\pm$ and the circled points are measured. Broken line is the calculated α_+/α_- and the triangles are measured points.

reverse absorption were measured and shown as discrete points in Figs. 15, 16 and 17. The polycrystalline YIG has $4\pi M = 1750$ oe at room temperature. Its linewidth ΔH was determined by measuring the dc magnetic fields at which the reverse isolator loss in db is one-half of the maximum. It is more than twice the usual linewidth. This is presumably due to the variation of the aspect ratio among the YIG disks and also partly due to the shape of the ferrite disks being square instead of ellipsoidal. The finger length of the structure was 0.198 inch but in the calculation of $\alpha_{\pm}$ it was assumed that $h = 0.22$ inch to correct for the fringe capacitance at the finger tips.

The ω-β relation of the comb structure was measured by a phase bridge technique described in the previous section. This makes it possible to relate ω to θ and also gives the group velocity.

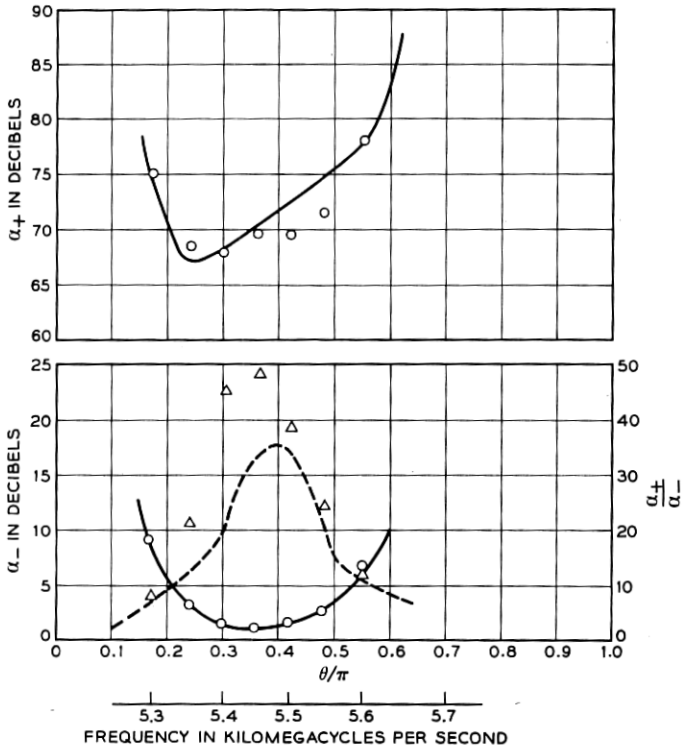

Fig. 16 — Measured and calculated forward and reverse absorption. Ferrite size: 0.02 × 0.02 × 0.002 inch (71 pieces). $L = 0.08$ inch, $D = 0.06$ inch, $l = 0.04$ inch, $a = 0.01$ inch, $\Delta H = 223$ oe, $4\pi M = 1750$ oe. Solid lines are the calculated $\alpha_{\pm}$ and the circled points are measured. Broken line is the calculated α_{+}/α_{-} and the triangles are measured points.

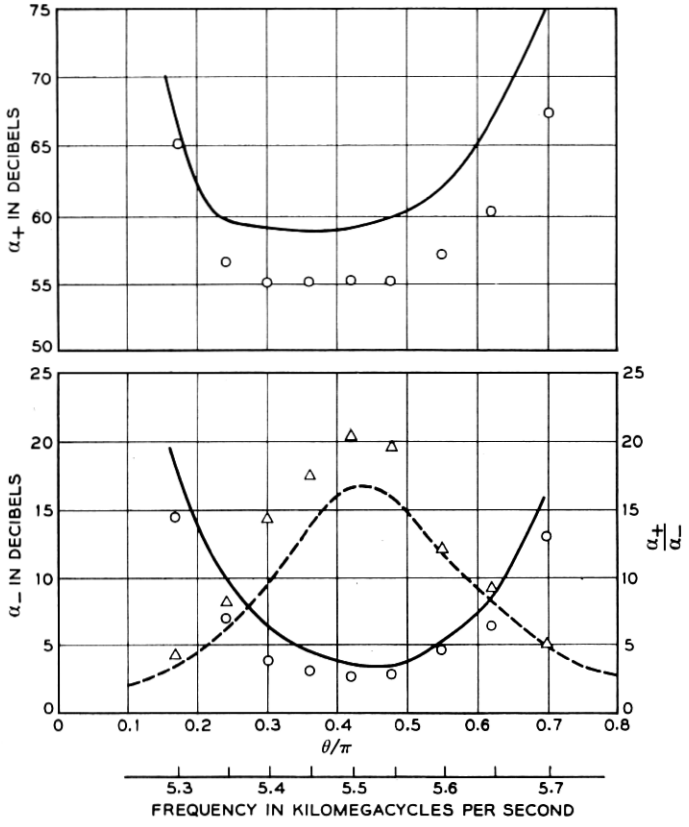

Fig. 17 — Measured and calculated forward and reverse absorption. Ferrite disks = 0.03 × 0.03 × 0.002 inch (35 pieces). L = 0.08 inch, D = 0.06 inch, l = 0.04 inch, a = 0.009 inch, ΔH = 251 oe, $4\pi M$ = 1750 oe. Solid lines are the calculated $\alpha_\pm$ and the circled points are measured. Broken line is the calculated α_+/α_- and the triangles are measured points.

Figs. 15 and 16 show the calculated and the measured data with 0.02 × 0.02 × 0.002 inch ferrite disks. Fig. 15 is for the case a = 0.016 inch and Fig. 16 is for a = 0.01 inch. The curves of Fig. 13 show that, by decreasing a from 0.016 to 0.01 inch, the reverse absorption increases more strongly at large θ than at small θ, and that the maximum value of α_+/α_- occurs at a smaller θ. These theoretical predictions are confirmed by the measurements, as can be observed from the data in Figs. 15 and 16.

The measured and the calculated $\alpha_\pm$ and α_+/α_- for the ferrite size of 0.03 × 0.03 × 0.002 inch are shown in Fig. 17. α_+ for the 71 pieces of ferrite disks was too large to be measured in our equipment. There-

fore every other ferrite disk was removed to reduce α_+ by half. Comparing the measured data shown in Figs. 16 and 17, one notices that, by increasing the size of the ferrite disk from 0.02 to 0.03 inch square, the reverse absorption α_+ increases about 1.6 times while the maximum isolation ratio α_+/α_- decreases by a factor of 2.4. These are approximately the values expected from the calculation.

The measurements agree well with the calculation in general. It should be mentioned that in calculating α_+, use was made of parameters which can be measured only within an accuracy of 10 per cent.

IV. CONCLUSIONS

It has been shown that the filling factor increases as the c axis of the ruby approaches the z axis of the structure for the usual 90° operation in ruby. The increase is more significant near the $\theta = 0$ end of the passband of the comb structure than near the $\theta = \pi$ end. For the forward-wave structure ($df/d\theta > 0$), this corresponds to larger increase of the filling factor near the lower cutoff frequency than near the upper cutoff frequency. The increase in F_p as the c axis of the ruby becomes parallel to the z axis of the structure is more pronounced at lower frequencies, since the transition probability of the spin is more linear at those frequencies.

The ratio of the reverse-to-forward absorption of the isolator incorporated in the TWM can be over a hundred if the size of the ferrite disks is very small compared to the width of the waveguide housing, $2D + d$, and the size of the fingers. At present, the isolation ratio is far from the best due to the necessity of using large-size ferrite disks to provide enough reverse absorption. The size of the ferrite disks can be kept small and yet provide a large reverse absorption if the imaginary part of the susceptibility of the ferrite, χ'', can be increased. Since at resonance $\chi'' = 4\pi M/\Delta H$, one should look for a material with a large $4\pi M$ and a smaller ΔH. The saturation magnetization, however, cannot be made arbitrarily large, since the dc magnetic field, which is fixed by the ruby resonance, must be greater than $4\pi M$ in order to saturate the isolator disks. ΔH of the ferrite should be about 20 oe, which is approximately the linewidth of ruby. ΔH of polycrystalline YIG at the temperature of 4.2°K is over 200 oe. This can be reduced to a certain extent by minimizing the scattering in the aspect ratios of the ferrite disks and the use of round disks instead of square disks, since the internal field of a round disk is more uniform than that of a square one. A single-crystal YIG with ΔH enlarged to about 20 oe

has good possibility as an improved isolator material for TWM application.

The analysis also shows that the isolation ratio gradually improves and then gets worse, while the reverse absorption steadily decreases, as the ferrite disks are moved away from the surface of the fingers toward the waveguide wall. Also, the optimum isolation ratio gradually shifts to a higher value of θ.

In order to provide enough reverse absorption, more than one isolator deck is usually stacked on top of another. It may seem as if the forward insertion loss of the isolator can be kept small over a wider range of θ if a composite isolator with different a's is used instead of one with the same a. However, by adding the curves of different a's in Fig. 12 one will find that this is not so.

The analysis and the curves provided in this paper enable one to estimate the increase in electronic gain obtained by a proper orientation of the c axis of the ruby and by the use of ruby slabs on both sides of the comb. The size of the ferrite disks necessary to provide sufficient isolation and the dependence of the isolator performance on the position of the ferrite disks are also discussed. Together with the Refs. 1 and 2, this paper constitutes part of an effort to reduce the experimental work involved in developing traveling-wave masers.

V. ACKNOWLEDGMENTS

We wish to thank W. J. C. Grant and M. Berry for the programming of the computation, and R. C. Petersen and R. P. Morris for their expert help in the measurements.

REFERENCES

1. Harris, S., DeGrasse, R. W., and Schulz-DuBois, E. O., Cutoff Frequencies of the Dielectrically Loaded Comb Structure as Used in Traveling-Wave Masers, B.S.T.J., **43**, Jan., 1964, p. 437.
2. Chen, F. S., B.S.T.J., this issue, p. 1035.
3. Schulz-DuBois, E. O., Paramagnetic Spectra of Substituted Sapphires — Part I: Ruby, B.S.T.J., **38**, Jan., 1959, p. 271.
4. Schiff, L. I., *Quantum Mechanics*, McGraw-Hill, New York, 1955.
5. Tabor, W. J., A 100-Mc Broadband Ruby Traveling-Wave Maser at 5 Gc, Proc. IEEE, **51**, August, 1963, p. 1143.
6. Dodd, D. M., Wood, D. L., and Barns, R. L., Spectrophotometric Determination of Chromium Concentration in Ruby, to be published.
7. Suhl, H., and Walker, L. R., Topics in Guided-Wave Propagation Through Gyromagnetic Media, Part I, B.S.T.J., **33**, May, 1954, pp. 579–659.